

ULTRA-HIGH SPEED SOLID-STATE FTIR SPECTROSCOPY AND APPLICATIONS FOR CHEMICAL DEFENSE

Tudor N. Buican*
Semiotic Engineering Associates LLC
Albuquerque, NM 87111

Arthur H. Carrieri
US Army RDECOM Edgewood Chemical Biological Center (ECBC)
Aberdeen Proving Ground, MD 21010

ABSTRACT

We introduce a new class of FTIR spectrometers capable of acquiring $6 \times 10^4 - 1.4 \times 10^5$ interferograms (spectra) per second, over the spectral range of $1 \mu\text{m} - 12 \mu\text{m}$, with a resolution of 10 cm^{-1} or better. The new FTIR technology is based on the use of birefringence interferometers and employs photoelastic modulators (PEMs) as birefringent elements for ultra-high modulation speed. With characteristic data rates of tens of kHz and wide spectral range, these spectrometers are eminently suitable for high-speed, spectrally detailed, chemical biological (CB) hyperspectral imaging.

1. INTRODUCTION

The concept of birefringence interferometry and its high-speed version based on PEMs were developed in the mid-80s (Buican, 1985; Buican, 1990; Buican and Martin, 1990; Buican, 1993). The novel and remarkable aspects of this technology are its insensitivity to vibrations and relative movements of the interferometer's optical components, and the extremely high frequencies at which interferogram data elements can be scanned (to more than 10^5 interferograms per second). The first prototype of an FT spectrometer based on a PEM birefringence interferometer was built in 1985 at the Los Alamos National Laboratory (LANL), winning an R&D-100 award in 1989. A subsequent commercial prototype spectrometer (1992) was used on a hyperspectral fluorescence laser-scan microscope (Buican et al., 1993).

We propose to extend our prior work in this field to the infrared region—a band most important for CB remote sensing and detection. We also propose that PEM-based FTIR technology is ideally suited for high-speed IR spectral analysis in a true real-time sense; in this spirit, the last section of this article presents several new CB detection technologies that will greatly benefit from the use of ultra-high speed PEM/FTIR spectrometry. These technologies include a panoramic infrared-imaging spectroradiometer (PANSPEC) for the hyperspectral imaging and detection of chemical clouds, and Thermal Luminescence (TL), a technique for standoff detection of contamination in water and on terrestrial surfaces.

2. PEM/FT SPECTROMETRY FUNDAMENTALS

This section gives a brief introduction to the theory of PEM/FT spectrometry and the first generation of PEM/FT spectrometers.

2.1 Birefringence Interferometry

In its simplest implementation (Fig. 1), a birefringence interferometer consists of a birefringent element placed between two polarizers (Buican, 1985, 1990; Buican and Martin, 1990). The optical axes of the birefringent element are at 45° relative to the direction of the polarizers.

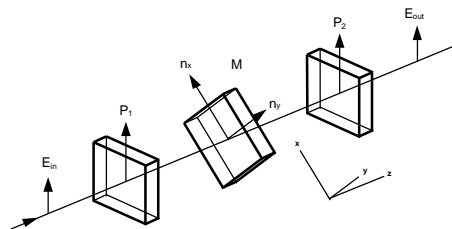


Fig. 1: The basic birefringence interferometer. E_{in} , E_{out} —input and output electric vectors; M—birefringence modulator; n_x , n_y —principal indices of refraction of the birefringence modulator and the corresponding optical axes; and P_1 , P_2 —polarizers and their optical axes.

A vertically polarized wave of amplitude E_{in} can be resolved into two components, along the optical axes x and y of the modulator, each of amplitude $E_{in} / \sqrt{2}$. A phase difference proportional to the retardation $x = l \Delta n$ ¹ is introduced between the two waves, where $\Delta n = n_x - n_y$ is the instantaneous modulator birefringence and l is the modulator thickness. For monochromatic waves of wavenumber $\sigma = 1/\lambda$, the phase difference is $\Delta\phi = 2\pi l \sigma \Delta n = 2\pi \sigma x$. By varying the modulator birefringence and therefore the retardation, an interferogram is generated as a function of the instantaneous

¹ Compare to $x = n \Delta l$ for a Michelson interferometer.

Report Documentation Page

Form Approved
OMB No. 0704-0188

Public reporting burden for the collection of information is estimated to average 1 hour per response, including the time for reviewing instructions, searching existing data sources, gathering and maintaining the data needed, and completing and reviewing the collection of information. Send comments regarding this burden estimate or any other aspect of this collection of information, including suggestions for reducing this burden, to Washington Headquarters Services, Directorate for Information Operations and Reports, 1215 Jefferson Davis Highway, Suite 1204, Arlington VA 22202-4302. Respondents should be aware that notwithstanding any other provision of law, no person shall be subject to a penalty for failing to comply with a collection of information if it does not display a currently valid OMB control number.

1. REPORT DATE 00 DEC 2004	2. REPORT TYPE N/A	3. DATES COVERED -			
4. TITLE AND SUBTITLE Ultra-High Speed Solid-State Ftir Spectroscopy And Applications For Chemical Defense		5a. CONTRACT NUMBER			
		5b. GRANT NUMBER			
		5c. PROGRAM ELEMENT NUMBER			
6. AUTHOR(S)		5d. PROJECT NUMBER			
		5e. TASK NUMBER			
		5f. WORK UNIT NUMBER			
7. PERFORMING ORGANIZATION NAME(S) AND ADDRESS(ES) Semiotic Engineering Associates LLC Albuquerque, NM 87111; US Army RDECOM Edgewood Chemical Biological Center (ECBC) Aberdeen Proving Ground, MD 21010		8. PERFORMING ORGANIZATION REPORT NUMBER			
9. SPONSORING/MONITORING AGENCY NAME(S) AND ADDRESS(ES)		10. SPONSOR/MONITOR'S ACRONYM(S)			
		11. SPONSOR/MONITOR'S REPORT NUMBER(S)			
12. DISTRIBUTION/AVAILABILITY STATEMENT Approved for public release, distribution unlimited					
13. SUPPLEMENTARY NOTES See also ADM001736, Proceedings for the Army Science Conference (24th) Held on 29 November - 2 December 2004 in Orlando, Florida., The original document contains color images.					
14. ABSTRACT					
15. SUBJECT TERMS					
16. SECURITY CLASSIFICATION OF:			17. LIMITATION OF ABSTRACT UU	18. NUMBER OF PAGES 8	19a. NAME OF RESPONSIBLE PERSON
a. REPORT unclassified	b. ABSTRACT unclassified	c. THIS PAGE unclassified			

retardation; its AC component (Buican, 1990) is given by

$$I_{out} = \alpha I_{in} \cos \Delta\varphi = \alpha I_{in} \cos(2\pi l\sigma \Delta n) , \quad (1)$$

where I_{in} and I_{out} are, respectively, the intensities of the incident and emerging radiation.

2.2 PEM/FT Spectrometry

Photoelastic modulators are essentially harmonic mechanical oscillators driven at resonance that exhibit a harmonic time dependence of the birefringence, $\Delta n = B \sin(\omega_0 t)$, where B is the birefringence amplitude and ω_0 is the angular frequency of mechanical oscillation. Then, the interferogram in Eq. (1) becomes

$$I_{out}(t) = \alpha I_{in} \cos[2\pi X\sigma \sin(\omega_0 t)] , \quad (2a)$$

and, for polychromatic light of intensity spectrum $I_{in}(\sigma)$,

$$I_{out}(t) = \alpha \int_0^{\infty} I_{in}(\sigma) \cos[2\pi X\sigma \sin(\omega_0 t)] d\sigma , \quad (2b)$$

where $X = lB$ is the retardation amplitude of the PEM. The phase of the interferogram in Eq. (2a) varies according to a sine law (Fig. 2a). This results in a simple distortion of the interferogram, whose phase changes

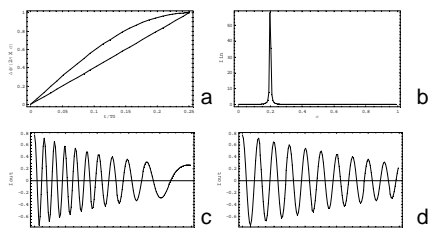


Fig. 2: Phase scanning. Linear and sine law phase scanning (a); narrow-band spectrum (b); sine law interferogram (c); and linear law interferogram (d). Arbitrary units are used in panels b, c, and d.

fastest at the origin and with a vanishing speed near the end of stroke (Fig. 2c). A standard interferogram, whose phase changes uniformly in time, is shown in Fig. 2d. Both interferograms correspond to the narrowband spectrum in Fig. 2b.

The linear transform in Eq. (2b) is closely related to the standard cosine Fourier transform encountered in FT spectrometry. If the sampling points of the interferogram are separated by constant phase increments², then the sampled interferogram can be processed with the standard numerical tools of FT spectrometry. If a uniform sampling clock is used, the phase distortion of the interferogram can be compensated for exactly by

² Such a sampling clock can be easily generated by separately monitoring the interferogram for a short wavelength probe laser beam through the interferometer.

introducing an identical distortion in the cosine kernel of the inverse transform. An additional weighting function in the inversion kernel compensates for the nonuniform phase increments, as shown in the following expression:

$$I'_{in}(\sigma) = \beta \int_0^{\tau_0/4} I_{out}(t) \cos[2\pi X\sigma \sin(\omega_0 t)] \cos(\omega_0 t) dt \quad (3)$$

The spectral resolution is the usual $1/X$ (Davis et al., 2001). In our experience, a typical Hinds³ PEM can be driven to retardation amplitudes of 5-10 μm , which results in a spectral resolution for a *single* PEM of 10^3 cm^{-1} and a spectral sampling interval of 500 cm^{-1} . We have shown that (1) this kind of resolution is eminently useful in the analysis and recognition of the broad but specific spectra encountered in molecular fluorescence (see Subsection 2.3); (2) methods exist for increasing the overall resolution by at least two orders of magnitude, at which point a PEM/FT spectrometer becomes competitive with, and in certain important applications preferable to, other spectrometer designs (see Subsection 3.3); and (3) the (sustained) rate of spectral acquisition using, for example, off-the-shelf PEMs operating at 30 KHz, is 120,000 interferograms/s (8.3 μs per interferogram), and 60,000 interferograms/s (16.7 μs per interferogram) if the spectral resolution is doubled by static phase.

2.3 First Generation Instruments

First generation PEM/FT spectrometers use either single PEMs or multiple PEMs without the special driving and control systems described in Section 3. In our experience, simple PEM stacks often result in poorer performance than a properly driven single PEM. This is a consequence of unavoidable variations in operating frequency among PEMs and of the temperature dependence of PEM resonance frequency; however, as we show in Section 3, it is precisely the latter phenomenon that can make stacked PEMs work efficiently.

Typically, a first generation PEM/FT spectrometer is mainly suited for the analysis of molecular fluorescence. As discussed Section 2.2, interferogram acquisition times for PEM/FT spectrometers are of the order of 10 μs . Therefore, they are well suited for monitoring fast transients and for hyperspectral imaging. Both applications are illustrated in Fig. 3 by FTCS-1 (R&D-100 winner in 1989), a flow cytometer using a PEM/FT spectrometer to analyze in real time the spectrum of the fluorescence emitted by single biological cells passing through a laser beam (Buican, 1985; Buican and Martin, 1990; Buican and Yoshida, 1992); and FT-1000, a hyperspectral imaging attachment for a laser-scan confocal microscope (Buican, 1990; Buican and Yoshida, 1992; Buican et al., 1993). Both systems achieved spectral

³ Hinds Instruments, Inc., 3175 N.W. Alcock Dr., Hillsboro, OR 97124-7135.

resolutions of about $1,500\text{ cm}^{-1}$. A diagram of the optical system of FT-1000 is shown in Figure 4.



Fig. 3: Two prototype instruments incorporating ultra-high speed FT spectrometers: a flow cytometer, FTCS-1 (left), and a hyperspectral imaging laser-scan confocal microscope, FT-1000 (right).

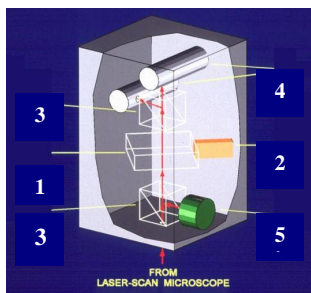


Fig. 4: FT-1000 PEM/FT Spectrometer. 1—Photoelastic modulator element; 2—Piezoelectric driver; 3—Polarizing beamsplitters; 4—Photomultipliers⁴; 5—Wavelength calibration diode laser.

2.4 PEM/FT Real-Time Data Processing

Both systems described in the previous subsection incorporate real-time parallel data processors. The analog interferogram signal is converted into a continuous digital data stream, which is sent over a private bus, together with PEM (and scanner on FT-1000) phase reference information, to all the processor modules. Each processor computes one transform element by accumulating the scalar products between successive interferograms and locally stores sets of coefficients (channel-specific digital spectral characteristics). Each processor in FT-1000 incorporates its own frame buffer, in which the sums of products are written for each pixel in synchrony with the scanning laser beam. This approach allows digitally filtered hyperspectral images to be generated in real time, as the sample is scanned by the probe laser. Figure 5 shows results obtained with FT-1000. Here, two fluorescent probes, fluorescein and propidium iodide (PI), were used to label biological cells. As fluorescein binds to proteins and PI to DNA, staining with these dyes can reveal the distinct spatial distribution of proteins and DNA in a cell. While similar spectrally resolved images can be obtained with optical filters, digital spectral

chemical imaging requires no sample-specific optical filters and works with large numbers of simultaneous arbitrary spectra.

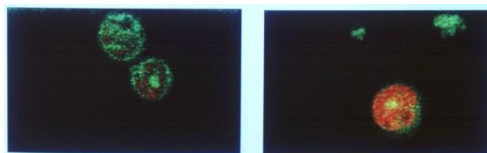


Fig. 5: Fluorescence-based hyperspectral chemical imaging with FT-1000. Real-time generated image from the “green” (fluorescein) channel (left), and two-color superposition of the images from the “green” and “red” (propidium iodide) channels (right).

On both systems, the control computer could also perform principal component analysis (PCA) on a set of raw interferograms. The resulting eigenspectra could be downloaded to the individual real-time processors, and more samples could then be analyzed. This is essentially a form of blind separation/generation of chemical contrast.

Section 4 presents potential chemical defense applications of the PEM/FT technology in the IR. Whether involving the analysis of fast spectral transients or hyperspectral imaging, these applications have front-end data acquisition and processing requirements that are similar to those illustrated in this subsection.

3. SECOND GENERATION PEM/FT SPECTROMETRY

As shown above, the spectral resolution and thus the usefulness of first generation PEM/FT spectrometers are limited by the maximum retardation achieved by available PEMs and driving electronics. The obvious solutions to this limitation are (1) to increase PEM driving amplitude; and (2) to stack multiple PEMs. A significant increase in total retardation requires the combined use of both approaches. However, as mentioned in Subsection 2.3, PEM-to-PEM variability and the temperature dependence of the PEMs' resonant frequencies mean that stacks are very inefficient. To make the stacked PEMs operate in phase and thus be able to add up the full individual PEM retardations, one must actively and continuously tune the PEMs to a common resonant frequency.

3.1 Dynamic PEM Model

A driven PEM generates heat. Its temperature consequently rises and its resonance frequency and driving efficiency change, causing the rate of heat dissipation to change and thus creating a thermal feedback mechanism that can lead to instabilities. We created a very simple model for the thermal feedback mechanism, which not only explained observed driving instabilities, but also allowed us to design digitally controlled, high-amplitude drivers that are both stable and continuously tunable. In our model, the PEM's internal temperature is governed by the simple first-order dynamics of capacitor

⁴ A polarizing beamsplitter allows two output beams with opposite interferogram phases to be produced. In this case, the interferogram signal is the analog difference between the intensities of these beams.

charging, where the lumped heat capacity of the PEM is “charged” by the sum of the internally dissipated heat flux and the heat exchanged with the environment through a lumped thermal resistance. The internal heat source is the heat dissipated by the lossy mechanical oscillator consisting of the resonant PEM and its piezoelectric driver(s).

The internal heat source is modeled as a lossy resonator described by its quality factor Q , resistance at resonance R , and (temperature-dependent) resonance frequency ω_0 . The resonator is driven by a sinusoidal voltage of amplitude V and angular frequency ω , which is eventually converted to a heat flux P_{th} . Finally, we assume a simple linear dependence of the resonance frequency on the internal temperature. The model leads directly to an equation for the rate of change of the resonance frequency (and internal temperature). Hence, a description of the steady-state behavior of the model is easily derived as an algebraic equation. At a given ambient temperature, this equation describes a surface (which we call the control surface) in the space of the driving parameters and the steady-state resonance frequency, as shown in Figs. 6a and 6b. One immediately notices that the surface is folded and that there is a

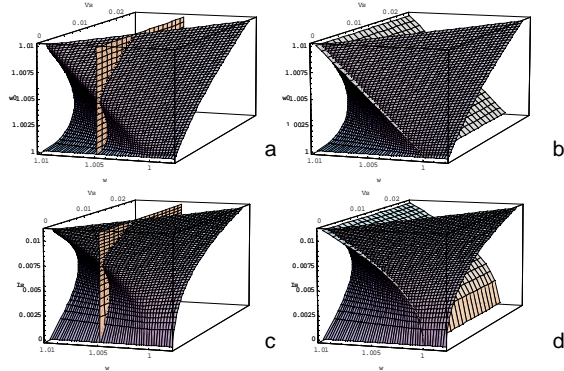


Fig. 6: Steady-state dependence of PEM resonance frequency (a, b) and PEM current (c, d) on driving voltage and frequency. A constant driving frequency plane is also shown in panels a and c, illustrating the existence of multiple steady-state values of the resonant frequency and current; and the resonance loci are shown in panels b and d, illustrating the smooth and monotonic behavior of the system when driven at steady-state resonance.

domain in the driving plane $\{V, \omega\}$ in which there are three possible steady-state values of the resonance frequency. One can show that the intermediate value is unstable, while the other two are stable. One can also see that the folding begins very close to the ambient temperature, and thus the instability manifests itself even at low driving levels. Furthermore, one can see that the fold at the lower values of the driving voltage is very close to the resonance driving condition (Figs. 6b and 6d), where $\omega = \omega_{0st}$. Thus, any PEM that is driven at or near resonance is within the region of instability.

Figures 6c and 6d. show the steady-state amplitude of the current through the PEM as a function of driving voltage and frequency. This parameter exhibits the same behavior as the resonant frequency. The graphs in Fig. 6 show that a PEM driven near resonance at a constant driving frequency (or one that changes slowly) is unstable. However, if the driving frequency is locked to the PEM’s instantaneous oscillating frequency, the resulting steady-state resonance operation is stable and the PEM current can be smoothly controlled by adjusting the driving voltage. We have designed and tested a novel PEM driver/controller system based on these results, as illustrated in Fig. 7. The driver (Fig. 7a) is a very robust solid-state high voltage (HV) switch with built-in high-speed current limiters that protect the system in case of component failure in the PEM. The switch generates a HV square waveform which is used to drive the PEM.

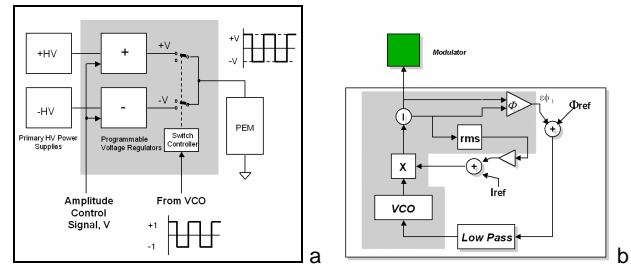


Fig. 7: Second generation PEM driver and controller. The driver (a) is an HV MOSFET switch driven by the output of the PLL VCO. The HV levels are adjusted by programmable voltage regulators. The driver, denoted by X, is connected to a local controller (b). See Fig. 10 for a prototype implementation.

The square, rather than sinusoidal, waveform does not affect the performance of the PEM, which typically has a quality factor Q in excess of 1000 and thus responds only to the fundamental frequency, which is close to its resonance frequency. The voltage amplitude of the driving signal is very simply controlled by two programmable voltage regulators, which set the voltages between which the PEM is switched.

A diagram of the local controller is shown in Fig. 7b. Operation at or near resonance is ensured by a phase-lock loop (PLL) which compares the phases of the drive voltage and current, and locks the former to the latter. The phase error drives a local voltage controlled oscillator (VCO), which in its turn drives the HV switch. A programmable phase shift Φ_{ref} can be introduced into the PLL circuit as a shift added to the phase error. When the phase shift is zero, the driving voltage waveform locks in phase to the current through the PEM. This phase condition corresponds to resonance, and, as a result, the PEM is driven at its characteristic resonance frequency. The system can be actively tuned over a range of a few widths of the resonance peak (several Hz to several tens of Hz depending on PEM type) simply by locking the driving voltage to the PEM current with a nonzero phase difference. Indeed, when the phase-locked driving voltage

is forced to trail the PEM current, the effective “resonant” frequency of the system (PEM and controller) settles to the value below the natural resonance that corresponds to the locked phase difference. When the driving voltage leads, the opposite effect occurs. The result is a robust, compact PEM system (Fig. 8) that is actively tuned by an external voltage.

3.2 Advanced PEM Stack Driving

The control system presented in Subsection 3.1 can be extended to multiple PEMs. This finding is a significant breakthrough because available single PEMs are not capable of providing the retardation amplitude required for FTIR spectrometry applications.

Resonant PEMs have very narrow resonant peaks (Q of the order of 10^3 to 10^4), and it is extremely difficult to tune multiple modulators to have overlapping resonance peaks, let alone identical resonant frequencies. Consequently, if multiple PEMs are driven at the same frequency, only one PEM (the master) runs exactly at resonance, while the remaining PEMs are driven off-resonance and thus oscillate with different phases; the resulting total amplitude is thus less than the sum of the amplitudes of the individual modulators.

In driving multiple PEMs, we use the temperature dependence of the resonant frequency to achieve *active, continuous, collective self-tuning* of the individual PEMs to a common resonant frequency. Self-tuning is achieved by the local control circuits of each PEM, which adjust the local driving voltage and, therefore, the steady-state temperature in such a way that each PEM resonant frequency moves toward the global driving frequency. Furthermore, the global control circuits adjust the global driving frequency so that it tracks an “average” resonant frequency. Thus, if multiple PEMs exhibiting a certain spread of resonant frequencies start at room temperature, the following will happen: (1) The global control circuits will set the driving frequency at the “center” of the resonant frequency spread; (2) the local control circuits will move the resonant frequencies of their respective PEMs toward the global driving frequency. Within the thermal time constant of the PEMs, the common driving frequency and the spread of resonant frequencies will collapse to a single value. From this point on, all the modulators are locked at a common resonance, oscillate with the same phase, and track together any change in the common resonant frequency that may be caused by changes in total amplitude. It should also be noted that, by indirectly including the individual PEM temperatures in the feedback loops, the total modulator amplitude becomes independent of changes in ambient temperature, as well as of differences in temperature among PEMs.

Another novel feature of our approach to driving multiple PEMs is that the total amplitude of the system can be regulated while, simultaneously, keeping the

PEMs locked at a common resonance. Furthermore, the time constant for amplitude regulation can be made much shorter than the thermal time constant. We achieve this result through “floating-amplitude” control (FAT). In this technique the individual PEM amplitudes are *not* actively regulated. Instead, the total amplitude is regulated, while the individual PEM amplitudes are allowed to float to individual levels consistent with the set total amplitude and the requirement for common resonance. While this may appear to lead to some level of operational uncertainty, the result is the opposite because there are sufficient constraints in the system to force the individual amplitudes to unique values.

3.3 Second Generation PEM/FT Technology Development

We have already demonstrated the driving and control principles presented in Subsection 3.1. with a system that employs fused silica PEMs. We are currently developing and testing a PEM/FTIR prototype that demonstrates that three ZnSe PEMs (Figures 8, 9) can be driven efficiently using the techniques presented in

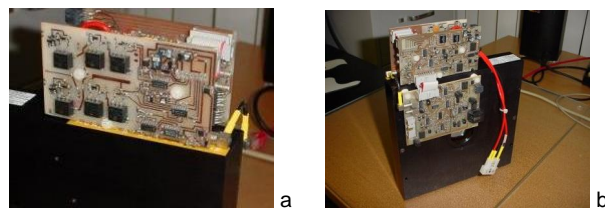


Fig. 8: Second generation PEM driver/controller. The modular driver and controller is mounted directly on a ZnSe IR PEM. The HV switching driver is shown in (a). The local controller board (top) and the communication interface board (bottom) can be seen in (b).

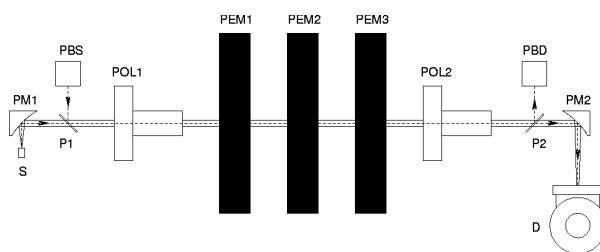


Fig. 9: PEM/FTIR development system. D—HgCdTe IR detector; P1, P2—ZnSe plates; PBD—Probe beam detector; PBS—Probe beam source; PEM1-PEM3—ZnSe PEMs; POL1, POL2—ZnSe polarizers; PM1, PM2—Off-axis parabolic mirrors.

Subsection 3.2. This project aims at reaching a total retardation of the order of $30 \mu\text{m}$ in the IR. This would indicate that a resolution better than 10 cm^{-1} can be achieved by the proposed prototype illustrated in Fig. 10 (Buican, 1997). This system represents the next stage in the development of PEM/FTIR technology and extends the technology demonstrated by the existing prototypes in

order to achieve the level of performance described in Table 1.

The novel features in this proposed design aim at improving the spectral resolution to a level consistent with most IR spectroscopy applications. We propose to achieve this by stacking ten PEMs; passing the beam ten times through this stack; and, finally, by doubling the retardation amplitude through a static birefringent element. Additionally, a uniform phase (rather than time) increment clock is used (see footnote 3).

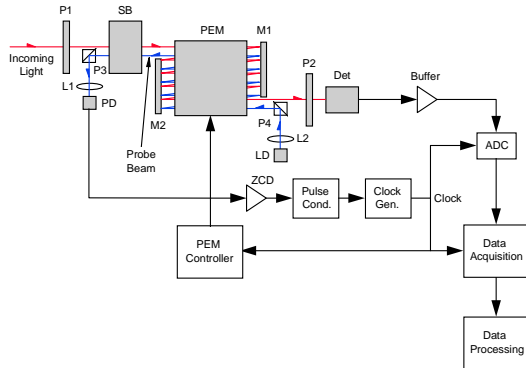


Fig. 10: Simplified block diagram of a PEM/FTIR spectrometer. ADC—analogue-to-digital converter; Det—mid-IR detector; L1, L2—lenses; LD—laser diode; M1, M2—path-folding mirrors; P1, P2—mid-IR polarizers; P3, P4—near-IR polarizing beam splitters; PD—near-IR photodetector; SB—static birefringent element; and ZCD—zero-crossing detector. The incoming light is shown in red, while the probe beam is shown in blue.

Once it has been developed to the level of the proposed prototype, PEM-based FTIR technology is ideally suited for high-speed, high-sensitivity, IR spectral analysis and hyperspectral imaging. The unique combination of spectral range (from the visible to the middle infrared), real-time spectrum acquisition rate (7×10^4 – 14×10^4 interferograms/spectra per second), spectral resolution (to 10 cm^{-1} and better) and useful clear aperture (10 mm) attainable by a PEM-based FTIR spectrometer are well outside the performance domain of competing technologies. Indeed, no other technologies match the full combination of parameters describing the proposed PEM/FTIR. Thus, (1) liquid crystal tunable filters (LCTF) are slower by 3-5 orders of magnitude in terms of scanned spectra per second, while also having lower light throughput; (2) acousto-optical (AO) tunable filters are slower by an order of magnitude and tend to have lower light throughput at comparable spectral resolution; they may also require higher driving power than PEM/FTIRs; (3) Fabry-Perot tunable filters exhibit much narrower spectral ranges, have poorer light throughput, and are considerably slower unless miniaturized (MEMS-based), in which case they cannot be used for imaging; (4) rotating mirror or prism FTIRs are at least two orders of magnitude slower in terms of scanned interferograms per second; (5) vibrating mirror Michelson FTIRs are 2-3

orders of magnitude slower; and (6) surface plasmon tunable filters—an emerging technology—would result, even when perfected, in spectrometers that are slower by at least an order of magnitude. Such filters are also currently limited to the near IR, although this limitation will likely disappear.

TABLE 1. Specifications for a feasible PEM/FTIR spectrometer

Spectral Range	From $\approx 5 \mu\text{m}$ to $\approx 12.5 \mu\text{m}$ ($800\text{--}2000 \text{ cm}^{-1}$)
Spectral Resolution	2.5 cm^{-1}
Light Throughput to Detector	3%–8%, for collimated, unpolarized light
Maximum Interferogram Bandwidth	$\approx 94 \text{ MHz}$
Probe-Beam Interferogram Bandwidth	$\approx 188 \text{ MHz}$
Sampling Points per Interferogram	≈ 800 , nonuniform sampling
Maximum Sampling Frequency	$\approx 188 \text{ MHz}$
Interferogram Scanning Time	$13.5 \mu\text{s}$
Interferograms Scanned per Second	74,000
Input Beam Diameter	$\approx 5 \text{ mm}$
PEM Frequency	37 kHz
PEM Windows	10
Detector	Photovoltaic HgCdTe, at 77 K

The unique combination of spectral range (from the visible to the middle infrared), real-time spectrum acquisition, spectral resolution, and useful clear aperture (10 mm) attainable by a PEM-based FTIR spectrometer is well beyond the performance domain of competing technologies.

4. APPLICATIONS FOR CHEMICAL DEFENSE

In military defense, remote sensing, and civil cleanup operations it is often vital to rapidly determine the occurrence and extent of atmospheric, land, and waterway CB contamination caused by deliberate release (as in the case of a detonated projectile) or accidental spill (as in the case of discharge from an industrial plant). The liquid/vapor/aerosol contaminant mass can be neutralized and life and health safeguarded most effectively once land/volumetric maps are in hand outlining the presence and quantity of these specific analytic compounds in situ. We present in this section two novel high-performance remote sensing technologies, which operate best at IR spectrum acquisition speeds made possible by the PEM/FT technology.

4.1 Hyperspectral Imaging with PANSPEC

PANSPEC (Panoramic Infrared-Imaging Spectroradiometer) is a computer-optimized spectroradiometer design for monitoring a panoramic infrared environment

for the presence of chemical clouds, and for tracking such clouds (Carrieri, 1997a, 1997b, 2003). It combines PEM/FTIR and photopolarimeter technologies, and integrates a wide-angle camera in forming a unified passive imaging remote sensor and active laser beacon system (Figure 11). The purpose of PANSPEC is to provide for a standoff detection capability of disseminated chemical weapons⁵; specifically, (1) detection of gaseous chemical warfare agents in the atmosphere to a range of approximately 50 km (a figure of merit for prototype construction); (2) tracking of the targeted hazardous cloud mass over a panoramic field of view (FOV); and (3) omnidirectional communications of cloud presence and heading by means of an encrypted laser beam carrier, projected into the exact panorama from which imaging is done.

As a sensor fusion concept, the 'heart' of PANSPEC is structured from a common configuration of three (or more) PEMs positioned between linear polarizers. The fusion of optics (Fig. 11) is required for joint infrared

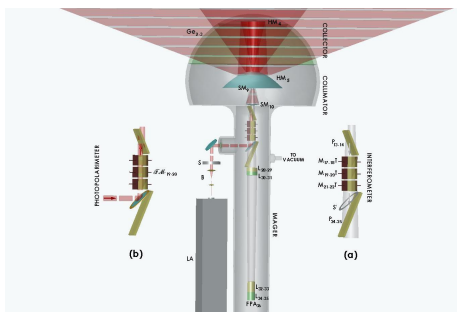


Fig. 11: The PANSPEC model in (a) passive interferometer and (b) active photopolarimeter modes of operation: HM: hyperboloid mirror; SM: spherical mirror; Ge: Germanium shell; MT : 1/2 and 1/4 waveplate sequencing of ZnSe crystal with transducer , P: linear polarizer; L: lens; FPA: focal plane array; LA: infrared continuous-wave laser; B: beam expander; S: shutter; and S': shutter with mirrored face on slide.

detection and communication performances by the same instrument, in an alternate manner (a novelty of the PANSPEC system). The linear optical array of 3 PEMs performs passive thermal FTIR spectrometry on throughput infrared radiance collected and collimated over the instrument FOV, and then imaged onto a focal plane array (FPA) of $n \times n$ pixel elements (eye toward the sky). The FPA simultaneously generates n^2 interferograms, one for each pixel element of the array, that are rapidly acquired via a parallel architecture analog-to-digital converter (ADC). These interferogram data records are subsequently transformed at full speed into infrared spectra by a real-time DSP frontend and subsequently analyzed by a neural network processor multiplexed to the

data processing frontend (Carrieri and Lim, 1995). The neural network performs pattern recognition of the chemical cloud's absorption or emission band moiety from one pixel or a group of pixels in the FPA, as the cloud intercepts and proceeds across the sensor's panoramic FOV. Since the FPA pixel elements subtend contiguous solid angles in the FOV, volumetric location and heading of the chemical cloud can be discerned by mapping those localized pixels that yield its analytic fingerprint absorption or emission infrared spectrum.

A double polarization-modulation operation on a CO_2 laser beam makes PANSPEC act as an active photopolarimeter-based photonics communication system. The rationale for this beacon is to provide a simultaneous alert to friendly forces located within the sensor FOV (fore, aft, and to the side of PANSPEC) of oncoming and/or outgoing chemical vapor threat events. A properly configured optical receiver (portable, mounted to an aircraft fuselage or onto a land vehicle, etc) staring at PANSPEC and within its semi-solid cone FOV can be made to detect the laser light. Broadcasting in PANSPEC commences on stand down of its interferometry mode and activation of its beacon mode. Thereupon, PANSPEC transmits stored detection/identification and heading data uncovered by the interferometer on any absorbing/emitting chemical vapor mass, measured over the FPA, during a preceding passive spectral measurement timeframe. In this sense, the beacon is an omnidirectional carrier of strategic data. Beam encryption is in the form of a Mueller matrix. Any receiver with adequate optics (telescope, focusing system, detector element) staring at PANSPEC and equipped with the proper phase-sensitive detection electronics (with key) can decrypt the binary code of the carrier beam instantaneously (real-time alert).

4.2 Thermal Luminescence (TL)

TL is a technology aimed at solving the standoff detection problem of contaminated water reservoirs (Carrieri and Roes, 2001) and terrestrial surfaces and synthetic landscapes (Carrieri, 1990; Carrieri et al., 1999). In TL, the energy of an irradiating beam is absorbed into the target material, yet all manifestations of the incident beam are absent from the detected radiance. TL is the broad portion of infrared radiance that is liberated from the beam-irradiated zone of the target. The energy of the surface irradiation beam is outside the TL bandwidth, yet coincides with a relatively strong absorption cross-section: e.g., a magnetron beam source tuned to 2.45 GHz—the W-band microwave region coinciding with strong absorption into contaminated soil. By scanning the irradiated surface, the PEM/FTIR produces high-speed interferograms that are transformed into graybody spectra of the TL. Typical of most inhomogeneous dielectric materials, this graybody is a Gaussian-like distribution of spectral amplitudes spanning 7.14 - 14.29 μm wavelengths of the middle infrared region. It is during beam

⁵ The goals of the program are to establish sensitivity, spectral resolution, and stability design specifications for a future chemical vapor imaging, detection, tracking and alert system.

irradiation that a thermal gradient is produced at the surface of irradiation. It is most prudent to measure a difference-spectrum along the maximum gradient event, $\Delta S = S(v, B) - S(v, A)$, where v spans the PEM/FTIR interferometer's middle infrared detection bandwidth, and A and B are adjacent heating periods. Inside the thermal nonequilibrium heating period, a *detection window of opportunity* develops, and the absorption bands of contaminant is revealed in ΔS . These bands are quite strong provided the graybody envelope $S(v, t)$ shifts at maximum rate (i.e., the maximum gradient condition) and when the shift in amplitude and frequency between contiguous spectra $S(A)$ and $S(B)$ is slight (which is related to interferogram acquisition rate and quantity of interferogram co-additions). Figure 12 succinctly illustrates how surface contamination via TL sensing is conducted.

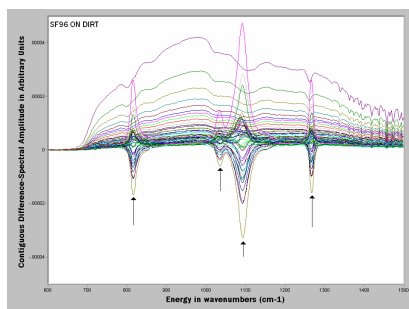


Fig. 12: The raw subtraction of TL contiguous spectra for soil slightly contaminated with SF96 (simulant of chemical nerve agent VX). SF96 is the polymer polydimethylsiloxane, with molecular vibrational modes indicated by the arrows. Polarity-reversal behavior of the molecular resonance bands is indicative of intermittent states of contaminant emission and absorption.

5. CONCLUSIONS

The outstanding spectral acquisition speed of a PEM-based FT spectrometer makes it the instrument of choice for real-time detection in the mid-IR. Indeed, this instrument could detect the presence of a new spectral signature within less than 100 μ s when used in conjunction with appropriate real-time data processing electronics. A PEM/FT spectrometer is also the ideal instrument for hyperspectral imaging applications. When used in conjunction with technologies such as PANSPEC and TL, PEM/FTIR could provide a considerable technological advance in chemical defense.

ACKNOWLEDGMENTS

This work was supported in part by the U.S. Army RDECOM Edgewood Chemical Biological Center (ECBC) under contract DABJ05-03-P-0979. Initial PEM/FTIR feasibility work was also supported by ECBC under contract DAAL03-91-C-0034. Initial work on advanced PEM driving and control (T.N.B.) was supported in part by Hinds Instruments, Inc.

REFERENCES

- Buican, T. N., 1985: Fourier Transform Flow Cytometry – The Interferometric Analysis of Emission Spectra from Individual Cells. *Proc. 11th Int'l Conf. of Analytical Cytology*, Hilton Head, SC, Intl. Soc. Analyt. Cytology.
- Buican, T. N., 1990: Real-Time Fourier Transform Spectrometry for Fluorescence Imaging and Flow Cytometry. *Proc. SPIE Symposium on Bioimaging and Two-Dimensional Spectroscopy*, Los Angeles, CA, SPIE, 126-133.
- Buican, T. N., 1993: Apparatus and Method for Measuring Fluorescence Intensities at a Plurality of Wavelengths and Lifetimes. US Patent No. 05208651.
- Buican, T. N., 1997: Feasibility Study for the Development of a High-Speed Fourier Transform Infrared (FTIR) Photoelastic Modulator (PEM) Based Spectrometer. Tech. Report to ERDEC, TCN Number 95-035, BTI, Albuquerque, NM, 53 pp.
- Buican, T. N., and J. C. Martin, 1990: Method and Apparatus for Simultaneously Measuring a Plurality of Spectral Wavelengths Present in Electromagnetic Radiation. US Patent No. 04905169.
- Buican, T. N., and T. M. Yoshida, 1992: Integrated Fluorescence Analysis System. US Patent No. 05117466.
- Buican, T. N., J. D. Harris, D. L. Neagley, S. Williams, T. Marks, and R. R. Bennett, 1993: FT-1000: A Fluorescence Spectral Imaging Microscope. *Proc. XVI Congress of ISAC*, Colorado Springs, CO., Intl. Soc. Analyt. Cytology.
- Carrieri, A. H., 1990: Infrared Detection of Liquids on Terrestrial Surfaces by CO₂ Laser Heating, *Appl. Opt.*, 29(33), 4907-4913.
- Carrieri, A. H., 1997a: Panoramic Infrared-Imaging Spectroradiometer Model With Reverse Phase-Modulated Beam Broadcasting, *Appl. Opt.*, 36(9), 1952-1964.
- Carrieri, A. H., 1997b: Earth Monitoring Satellite System with Combined Infrared Interferometry and Photopolarimetry for Chemical and Biological Defense, US Patent No. 5,659,391.
- Carrieri, A. H., 2003: Chemical Imaging Sensor and Laser Beacon, *Appl. Opt.*, 42(15), 2772-2784.
- Carrieri, A. H., and Lim, P. I., 1995: Neural Network Pattern Recognition of Thermal-Signature Spectra for Chemical Defense, *Appl. Opt.*, 34(15), 2623-2635.
- Carrieri, A. H., and Roese, E. S., 2001: Thermal Luminescence Water Monitor, *Appl. Opt.*, 40(18), 2998-3004.
- Carrieri, A. H., Barditch, I., Owens, D. J., Talbard, M., Lim, P. I. and Roese, E. S. 1999: Thermal Luminescence Sensor for Ground Path Contamination Detection, *Appl. Opt.*, 38(27), 5880-5886.
- Davis, S. P., M. C. Abrams, and J. W. Brault, 2001: *Fourier Transform Spectrometry*. Academic Press, 262 pp.